THE ROYAL SOCIETY

Published online 31 July 2003

How to perform measurements in a hovering animal's wake: physical modelling of the vortex wake of the hawkmoth, *Manduca sexta*

Eric D. Tytell* **and Charles P. Ellington**

Department of Zoology, University of Cambridge, Downing Street, Cambridge CB2 3EJ, UK

The vortex wake structure of the hawkmoth, *Manduca sexta*, was investigated using a vortex ring generator. Based on existing kinematic and morphological data, a piston and tube apparatus was constructed to produce circular vortex rings with the same size and disc loading as a hovering hawkmoth. Results show that the artificial rings were initially laminar, but developed turbulence owing to azimuthal wave instability. The initial impulse and circulation were accurately estimated for laminar rings using particle image velocimetry; after the transition to turbulence, initial circulation was generally underestimated. The underestimate for turbulent rings can be corrected if the transition time and velocity profile are accurately known, but this correction will not be feasible for experiments on real animals. It is therefore crucial that the circulation and impulse be estimated while the wake vortices are still laminar. The scaling of the ring Reynolds number suggests that flying animals of about the size of hawkmoths may be the largest animals whose wakes stay laminar for long enough to perform such measurements during hovering. Thus, at low advance ratios, they may be the largest animals for which wake circulation and impulse can be accurately measured.

Keywords: vortex wake; circulation; turbulence; vortex ring evolution; particle image velocimetry

1. INTRODUCTION

Insects use a variety of techniques to increase the lift forces from their wings. All of these techniques, including the leading-edge vortex (Ellington *et al.* 1996) and wing rotation (Dickinson *et al.* 1999; Sane & Dickinson 2002), involve increasing the circulation around the wing. However, the importance of wing rotation has been questioned (van den Berg & Ellington 1997*a*; Sun & Tang 2002) and the contribution of the leading-edge vortex is difficult to assess without direct measurements of its strength (van den Berg & Ellington 1997*a*).

Measuring circulation in the wake of flying animals could help to resolve these questions about high-lift mechanisms. Modern quantitative flow visualization facilitates measurements of circulation, as well as force, work and power from living animals. However, even using these modern techniques, wing motion makes direct circulation measurements around a wing very difficult. Rather than performing measurements around the wing, vortex wake theories (Rayner 1979*a*,*b*; Ellington 1984*b*) predict that the circulation in the wake should match that around the wing. Even these simpler measurements are complex, though, and many methodological problems and intrinsic issues of wake development make accurate estimation difficult.

*Author and address for correspondence: Department of Organismic and Evolutionary Biology, Harvard University, 26 Oxford Street, Cambridge, MA 02138, USA (tytell@oeb.harvard.edu).

One contribution of 20 to a Theme Issue 'Modelling in biomechanics'.

Vortex theories (Rayner 1979*a*,*b*; Ellington 1984*b*) approximate the wake as a series of unlinked vortex rings: circular distributions of vorticity shed off the wings at every beat (figure 1). Producing circular vortex rings is the most efficient method for an animal to propel itself through a fluid (Lighthill 1973), and there is experimental evidence that rings do exist in the wake, although the distribution of vorticity may be more complex than the models assume (Spedding *et al.* 1984; Spedding 1986; Willmott *et al.* 1997). Application of the extensive theoretical and experimental work on vortex rings (reviewed in Shariff & Leonard 1992) could provide direct methods for estimating wake momentum, circulation and energy for flying animals. However, even for the simplified vortex wake structure, experimental studies have had difficulty in accurately measuring these values.

Flight experiments have used hovering or slow flight as a test case. In hovering, the impulse of a wake vortex ring, i.e. the total momentum imparted to the fluid during vortex ring generation, can be estimated directly from measurements in the wake. Since a hovering animal is stationary, all of the measured impulse I is used to support its weight. Therefore, the measured must be equal to the ideal impulse I_0, the animal's weight multiplied by the period of vortex ring generation

$$I_0 = \frac{mg}{f}, \tag{1.1}$$

where m is the mass of the animal, g is the acceleration due to gravity and f is the vortex ring generation frequency (equal to the wing beat frequency when weight support is provided only on the downstroke, and twice that value

DOI 10.1098/rstb.2003.1355

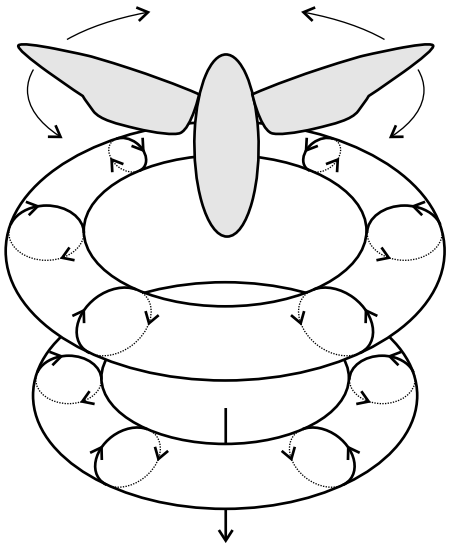

Figure 1. Schematic of two vortex rings in the wake of a hovering hawkmoth (after Ellington 1984*b*). The moth is shown in grey. Because Ellington's vortex wake theory is based on Rankine–Froude momentum jet theory (Ellington 1984*a*), the vortex ring radius is predicted to decrease in the far field, rather than increase, as was seen in this current study.

when the upstroke provides support as well). A mismatch between the measured and ideal impulses reveals potential inaccuracies in the wake measurements. For example, Spedding *et al.* (1984) and Spedding (1986) studied the wakes of slow-flying pigeons and jackdaws, but their wake impulse estimates were consistently lower than those necessary to support the birds' weights.

The *momentum deficit* common to these studies could come from two types of error: simple measurement errors, or intrinsic problems with the measurement of these types of wakes. Measurement errors may include insufficient sampling density, excess velocity error that obscures small vorticity fluctuations and spatial averaging from PIV. Intrinsic problems include, first, problems with the assumptions of the wake model, or, second, if the assumptions are correct, problems related to vortex ring dynamics that make measurements on circular vortex rings difficult.

For intrinsic errors, in the first case, the models assume that the wake consists of simple circular vortex rings and that force balances are in effect. However, the individual shedding events may have more complex vorticity distributions than simple circular vortex rings (van den Berg & Ellington 1997*b*) or the models may not correctly account for the dynamics of linked vortex rings.

If the models do describe the wake accurately, the dynamics of vortex ring evolution still makes measurement complicated. In theory, the total circulation of a vortex ring system stays constant unless it interacts with a solid body. In practice, though, measuring the circulation can be difficult or impossible, for two reasons: viscosity and turbulence. The more important of the two is determined by the ring Reynolds number *Re*, defined according to a dimensional argument (e.g. Glezer 1988) as

$$Re = \frac{UR}{\nu} = \frac{\Gamma}{\nu}, \tag{1.2}$$

where U, Γ and R are the ring velocity, circulation and radius, respectively, and ν is kinematic viscosity. For low Reynolds number rings, viscosity is the dominant force. It causes the vorticity in the rings' cores to diffuse out. In theory, this does not decrease the circulation, but it reduces the velocities in the rings by spreading them out over a larger area, which makes them harder to measure. High Reynolds number rings, by contrast, are not affected much by viscosity, but are unstable. They often develop azimuthal waves around their circumference, which eventually cause turbulence in the ring. The flow becomes more disorderly and the ring tends to shed vorticity. In theory, again, the circulation of the vortex ring and all of the pieces of shed vorticity remains constant. The vorticity shed by the ring, though, may be small enough to be affected by viscous vorticity diffusion, even if the ring itself is not. Shed vorticity may thus be hard to measure. Even worse, vorticity is also shed randomly, which means that a fluid element with one sense can interact with another of the opposite sense, cancelling both of them out and actually reducing the total circulation.

Despite these problems, it is still worthwhile to pursue the goal of accurately estimating flying parameters from the wake. Accurate *in vivo* measurements of thrust, circulation and power output in the wake of a flying animal could help to refine current high-lift models of insect flight, as well as other theoretical predictions, including estimates of optimal migration speed, maximum muscle power output and lift, thrust and drag (Pennycuick 1975; Casey & Ellington 1989; Ellington *et al.* 1996; Alexander 1997; Sane & Dickinson 2002). To perform these measurements accurately, this study seeks to determine the intrinsic causes of the momentum deficit and possible methods for avoiding the deficit. This study does not discuss measurement error in the PIV technique, which has already been analysed thoroughly (e.g. Huang *et al.* 1997; Westerweel 1997), and ultimately can be minimized. Instead, we focus on intrinsic errors. By artificially generating a wake similar to that of a hovering hawkmoth, the wake parameters can be precisely controlled and repeated, enabling direct comparisons of initial values and values estimated from the wake, which is impossible to do in a biological system. The sources of intrinsic error leading to the momentum deficit can thus be assessed and ultimately avoided.

2. MATERIAL AND METHODS

An artificial vortex ring generator was constructed to produce rings like those in a hovering hawkmoth's wake (Willmott & Ellington 1997*a*,*b*), assuming that weight support is provided only by the downstroke: that is, the frequency of ring generation equalled the wing beat frequency. Rings were generated by a piston moving rapidly through a sharp-edged 10 cm diameter tube, designed to match the hawkmoth's wingspan (*ca.* 10 cm) and disc loading, p_d (the force of the moth's weight divided by the area swept by its wings: *ca.* 3.0 N m^{-2}). From equation (1.1), the desired impulse, I_0, of the artificial ring is

$$I_0 = \frac{p_d A}{f}, \tag{2.1}$$

which must be equal to the total momentum I imparted to the fluid over the time during which the piston moves,

Table 1. Vortex ring generation parameters.

parameter		units	value
disc loading	p_d	N m^{-2}	3.0
generation frequency	f	Hz	25
correction factor	λ	—	4/3
stroke duration	T	ms	40
stroke length	L	mm	44.2
mean stroke velocity	U	m s^{-1}	1.10

$$I = \rho A L \lambda \overline{U}, \tag{2.2}$$

where A, L and $\overline{U}$ are the piston's area, stroke length and mean velocity, respectively, and λ is a correction factor that describes how much the piston deviates from its mean velocity (cf. P in Glezer 1988). The parameter λ is defined so that $\overline{\lambda U(t)^2} = \overline{U(t)}^2$, where the overbars denote a temporal average and t is time. In other words, λ corrects the square of the mean velocity to give the mean square velocity, which is proportional to the momentum imparted. Noting that the mean piston velocity $\overline{U}$ is Lf, and equating equations (2.1) and (2.2), we can solve for the stroke length

$$L = \frac{1}{f}\sqrt{\frac{p_d}{\lambda\rho}}. \tag{2.3}$$

Using the mean disc loading value of 3.0 N m^{-2} from Wilmott & Ellington (1997*b*), a generation frequency equal to the wingbeat frequency of 25 Hz and λ of 4/3 (representing a piston motion with constant acceleration followed by constant deceleration), the stroke duration, T, is 40 ms and the stroke length, L, is 44.2 mm, giving a mean stroke velocity of 1.10 m s^{-1}. Table 1 summarizes the generation parameters.

The initial circulation of the vortex ring can be estimated from these generation parameters. The rate at which vorticity is shed during the piston stroke is $\frac{1}{2}[U(t)]^2$. Integrating this expression over the stroke period to obtain the total circulation added to the fluid, the initial circulation Γ_0 is thus

$$\Gamma_0 = \frac{1}{2}\lambda L^2 f. \tag{2.4}$$

Didden (1979, 1982) directly measured the vorticity flux from a pipe vortex ring generator and found that the actual flux is slightly higher than equation (2.4) suggests, largely owing to boundary layer effects around the edge of the tube. Shariff & Leonard (1992) found that the initial circulation could be accurately predicted using the following corrected circulation $\Gamma_{0,c}$:

$$\Gamma_{0,c} = \left(1.14 + 0.64\frac{R}{L}\right)\Gamma_0, \tag{2.5}$$

where R is the pipe radius.

To produce these rings, a Ling Vibrator V201 was connected through a lever arm to a 10 cm diameter piston in a tube with sharp edges. This allowed stroke lengths of up to *ca*. 50 mm over 40 ms, producing a maximum generation impulse of *ca*. 1 mNs. The piston position was calculated from the vibrator position, monitored with a LVDT. Flow was visualized in a $2.1 \times 0.6 \times 0.6$ m glass chamber using smoke or polystyrene particles. The chamber was sealed and kept away from sources of heat to minimize convection. Smoke (vaporized mineral oil) was produced by a Nutem smoke generator and pumped into the vortex generator tube from two holes in its sides; particles (Expancel 091 DE 80 expanded polystyrene) were directly pumped into the chamber using a simple atomizer. A vertical laser light sheet, produced using a 6 mm rod lens with a 60 mW Omnichrome 532 argon ion laser, provided illumination. Care was taken to film at right angles to the light sheet using an Adimec MX12P digital CCD camera running at frame rates from 25 to 214 Hz, corresponding to resolutions of 1024×1024 to 1024×100 pixels (figure 2). Most images were filmed at either 80 or 100 Hz. Images were directly digitized using a Matrox Pulsar digitizer and Eye Image Calculator v. 2.0 (Io Industries) software. Different image sets were synchronized in time using an LED that was activated during the piston stroke.

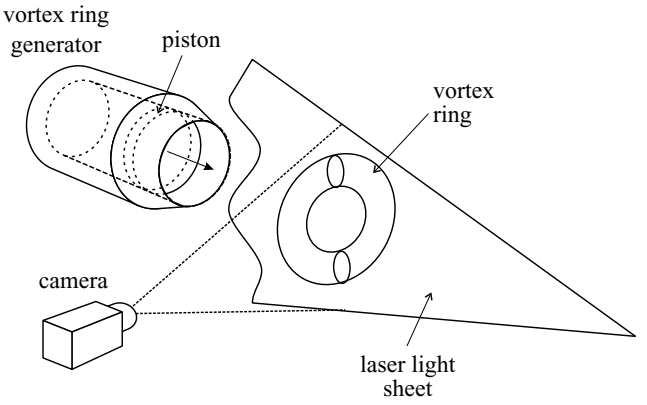

Figure 2. PIV filming configuration with a vertical light sheet.

Vortex ring position and diameter were calculated from the smoke images by manually identifying the vortex core using Matlab v. 5.0 (The MathWorks, Inc.). The spatial origin was defined as the end of the generator tube in x, and its axis in r (figure 2). The temporal origin was the end of the piston stroke. PIV, as described in Westerweel (1997), was performed on the particle images, with interrogation regions of *ca*. 24×24 mm (40×40 pixels) and grid spacing of 9×9 mm (15×15 pixels). Erroneous vectors were rejected manually only when both the magnitude and direction were noticeably different from their neighbours, and were replaced using a cubic spline interpolation. Data were taken from three rings, each at a different point along the ring path: at $x = 0$–0.5 m, 0.2–0.7 m and 0.8–1.3 m, corresponding to times $t = 0.3$–0.6 s, 1.0–2.4 s and 4.2–5.1 s. In the first region, the ring was laminar; in the second, it started the transition to turbulence; and in the third, it was turbulent.

The circulation of the vortex ring is the line integral of velocity around the vortex core, assuming that all vorticity is confined to the core. Based on this assumption, the outer contours can be placed at an arbitrary distance where fluid velocity is zero, and thus can be ignored. The only contour that matters, then, is along the centre-line. Because PIV is a discrete technique, circulation was calculated using a trapezoidal integration algorithm along the centre-line velocity profile, as in Spedding *et al.* (1984). The centre-line was identified manually and velocity vectors were linearly interpolated along it. Circulation values were rejected if the centre-line profile did not reach zero on both sides of the vortex ring. Circulation was not calculated by directly integrating around a circle enclosing the vortex core, because the image magnification was too high to visualize both the centre-line and the outer edges of the vortex core simultaneously.

Glezer & Coles (1990) describe another way to estimate circulation, but only for turbulent vortex rings. Using a similarity coordinate ξ and a normalized fluid velocity u_t^*, defined as

$$\xi = (x - x_0)\left(\frac{\rho}{I(t - t_0)}\right)^{1/4}$$

and

$$u_t^* = u\left(\frac{\rho}{I}\right)^{1/4}(t - t_0)^{3/4}, \tag{2.6}$$

the circulation can be estimated by an integral in time along one point in space:

$$\Gamma = \left(\frac{I}{\rho}\right)\frac{1}{(t - t_0)^{1/2}}G,$$

where

$$G = \int_0^\infty u_t^* \, \mathrm{d}\xi, \tag{2.7}$$

and where x_0 and t_0 are the apparent origins of the ring in space and time. The parameter G is constant during the life of the turbulent ring, and defines its 'strength,' much as the circulation Γ does for a laminar ring. Once G is known, the circulation for the turbulent ring can be estimated for any time after the transition to turbulence.

Glezer and Coles also formulate a set of proportionalities, as follows:

(i) $R \propto (x - x_0)$
(ii) $(x - x_0)^4 \propto (t - t_0)$
(iii) $U^{-1/3} \propto (t - t_0)^{1/4}$
(iv) $U^{-1/3} \propto (x - x_0)$,

where R is the vortex ring radius and U is its velocity. These relations can be used to estimate the apparent origin in space and time.

To assist comparisons with data from *Manduca* and other vortex ring studies, all variables were normalized. Following Weigand & Gharib (1997), we use dimensionless, normalized time t^* and vortex ring velocity U^* as follows:

$$t^* = \frac{\nu t}{16R^2}$$

and

$$U^* = \frac{4\pi UR}{\Gamma^0}, \tag{2.8}$$

where ν is the kinematic viscosity. In addition, a normalized vortex ring radius R^* and circulation Γ^* were used:

$$R^* = \frac{R}{R_0}$$

and

$$\Gamma^* = \frac{\Gamma}{\Gamma_0}, \tag{2.9}$$

where R_0 and Γ_0 are the tube radius and initial vortex ring circulation, respectively.

Once ring circulation is measured, the actual ring impulse I is

$$I = \rho\Gamma A, \tag{2.10}$$

where A is the area of the ring. This was then compared with the impulse produced by the vortex ring generator, estimated from equation (2.2).

All reported error values are standard errors of the mean. Where it is not obvious, n is also listed.

3. RESULTS

The piston stroke, although it deviated significantly from the ideal velocity profile, was repeatable. The piston position could be measured to 1% error. The mean velocity correction factor λ for all strokes was 1.261 ± 0.002 ($n = 56$). Despite the repeatability, though, vortex rings often had different paths and velocities. Most of the variation seemed to come from random turbulent shedding of vorticity.

Vortex rings were generated with two ranges of generation impulse values: one similar to that of hovering *Manduca*, 0.7–1.0 mN s ($Re = 4000$ to 5000), and a lower one for comparison, 0.4–0.45 mN s ($Re = 2800$ to 3000). At the higher impulse, the Ling vibrator was operating close to its maximum force output, causing the stroke duration to be less repeatable and increasing the range of generation impulses.

All vortex rings were initially laminar and became turbulent. There were four identifiable periods in the evolution of the rings (as in Sallet & Widmayer 1974; Weigand & Gharib 1994) as follows:

(i) an initial laminar phase, in which the ring appears smooth and circular;
(ii) the beginning of the azimuthal wave instability, in which waves are visible around the circumference of the ring, but it retains its smooth appearance;
(iii) the onset of turbulence, when the wave nodes become enlarged and the apparent circulation around them increases; and
(iv) a fully turbulent stage.

For both impulse ranges, the laminar period lasted for 1.5 ± 0.1 s, followed by a wave period of 0.3 ± 0.1 s and a turbulent onset period of 0.7 ± 0.1 s, after which the rings were fully turbulent. They generally travelled for eight to ten diameters before becoming turbulent, and up to the end of the tank (15 or more diameters further) after becoming turbulent. Transition times and positions were not significantly different for the different impulse rings ($p > 0.05$ in all cases).

Vortex ring radius stayed approximately constant during the laminar phase, and increased after the onset of turbulence (figure 3). Low-impulse rings had a lower normalized radius during the laminar phase, 0.764 ± 0.004 ($n = 8$), compared with that for high-impulse rings, 0.891 ± 0.001 ($n = 6$).

The velocity of the rings decreased during the laminar period (figure 4), but then varied greatly when they were turbulent (not shown). Figure 4*a* shows the difference between true velocities for high- and low-impulse rings; figure 4*b* shows how the velocity and time normalizations allow both impulses to be pooled. The high variance for the turbulent rings is owing to the difficulty of determining their positions. The laminar data were fit using a logarith-

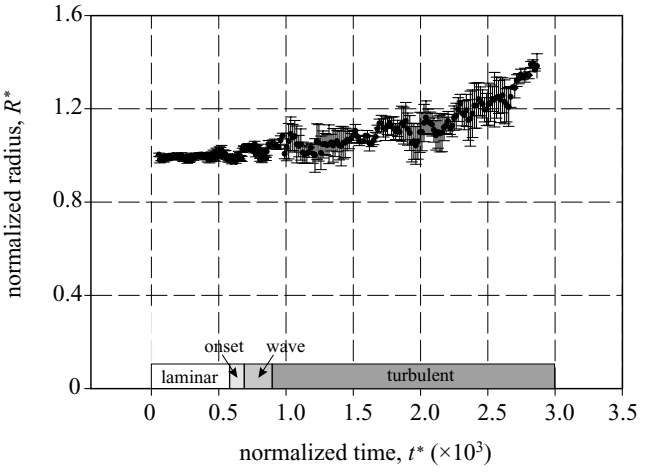

Figure 3. Normalized radius versus normalized time. Each point is the mean of at least two radii, and error bars indicate s.e.m. Azimuthal waves start at $t^* = 0.0005$, and turbulence begins at about $t^* = 0.001$. The bar at the bottom shows the state of the ring, from laminar to turbulent.

mic equation based on the model of Saffman (1970) of viscous vortex ring velocity

$$U^* = A \log t^* + C, \tag{3.1}$$

where A and C are constants estimated from the data. This model does not account for vortex ring formation or turbulence, and thus only values of between $t^* = 8 \times 10^{-5}$ and 7×10^{-4} were included in the fit. For this time period, $A = -0.43 \pm 0.04$ and C ranged from –0.6 to 1.5 ($n = 7$). The model of Saffman (1970) has $A = -0.5$; the estimated A value is not significantly different from this ($p = 0.18$). The value of C in his model (0.558) is derived by assuming an approximately solid body rotation in the core. The large range of estimated C values indicates that this assumption is invalid. The overall logarithmic decrease in velocity, though, suggests that these rings are significantly affected by viscosity.

To assess the feasibility of estimating circulation from vortex rings in air, PIV was conducted at three stages in the vortex ring evolution: early in the laminar period, during the transition to turbulence and during the turbulent period. Circulation was calculated for 40 frames from two laminar rings and 55 frames from one turbulent one. Only a few rings were analysed owing to the difficulty of attaining the proper particle seeding densities in air.

A sample velocity field and centre-line profile for a laminar ring is shown in figure 5. For laminar rings in the first two phases, the estimated circulation, 680 ± 9 cm^2 s^{-1}, was close to the initial circulation, 694 cm^2 s^{-1}, meaning that the normalized circulation Γ^* was close to unity: $\Gamma^* = 0.98 \pm 0.07$. After the transition to turbulence in the second phase, the estimated circulation had decreased to 560 ± 30 cm^2 s^{-1}, giving $\Gamma^* = 0.84 \pm 0.04$. Fully turbulent rings in the third phase had circulations of 393 ± 1 cm^2 s^{-1}, $\Gamma^* = 0.598 \pm 0.002$. Figure 6 shows the normalized circulation plotted versus normalized time.

The error in velocity values from the PIV algorithm was estimated by calculating velocities for still air. This produces a combined error that includes the imperfections in the video system as well as the accuracy of the PIV algorithm itself. It will, however, tend to highlight the tendency

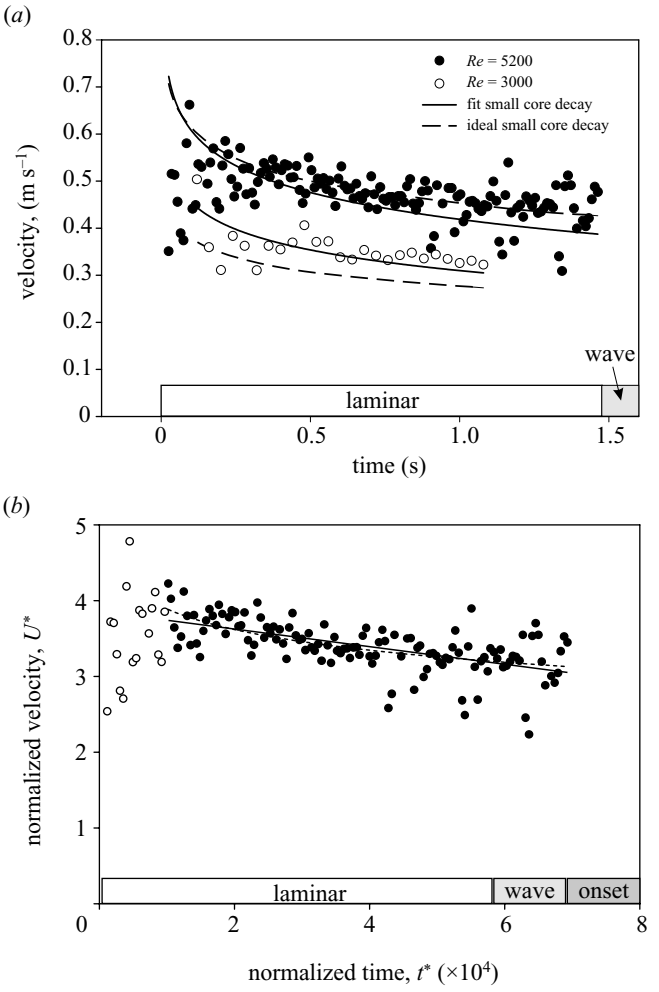

Figure 4. Velocity decreases logarithmically with time for laminar rings. Both plots have a bar at the bottom that indicates the state of the ring. (*a*) Plot of true velocity versus time for two rings of different Reynolds numbers, with the actual Saffman (1970) viscous decay model (dashed line) and a logarithmic model that accounts for deviations from solid body rotation in the vortex ring core (equation 3.1; solid line). (*b*) Pooled data for normalized vortex ring velocity with logarithmic (equation 3.1; solid line) and linear (dashed curve) fits. Only the filled points were used to calculate the fit, because the logarithmic model is not valid at small times.

for PIV to produce integer pixel displacements (G. R. Spedding, personal communication; for a general discussion of PIV errors, see Huang *et al.* 1997; Nogueira *et al.* 1997). The mean velocity estimate in still air was not significantly different from zero ($p = 0.4$) and the mean magnitude, equal to the error on velocity measurements, was less than 0.4 cm s^{-1}. Given this error on velocity, the circulation estimates had a total error of 16 cm^2 s^{-1}, or *ca.* 2% (Taylor 1982). The larger errors above seem be a result of true variations between vortex rings.

For the turbulent rings, circulation was also estimated using the Glezer & Coles (1990) transform. First, the apparent origin was calculated using the proportionalities above. The apparent spatial origin x_0 was estimated according to (iv) by fitting $U^{1/3}$ to x. The temporal origin t_0 was estimated with (ii), by fitting $(x - x_0)^4$ to t. The scatter in the data resulted in large errors on both esti-

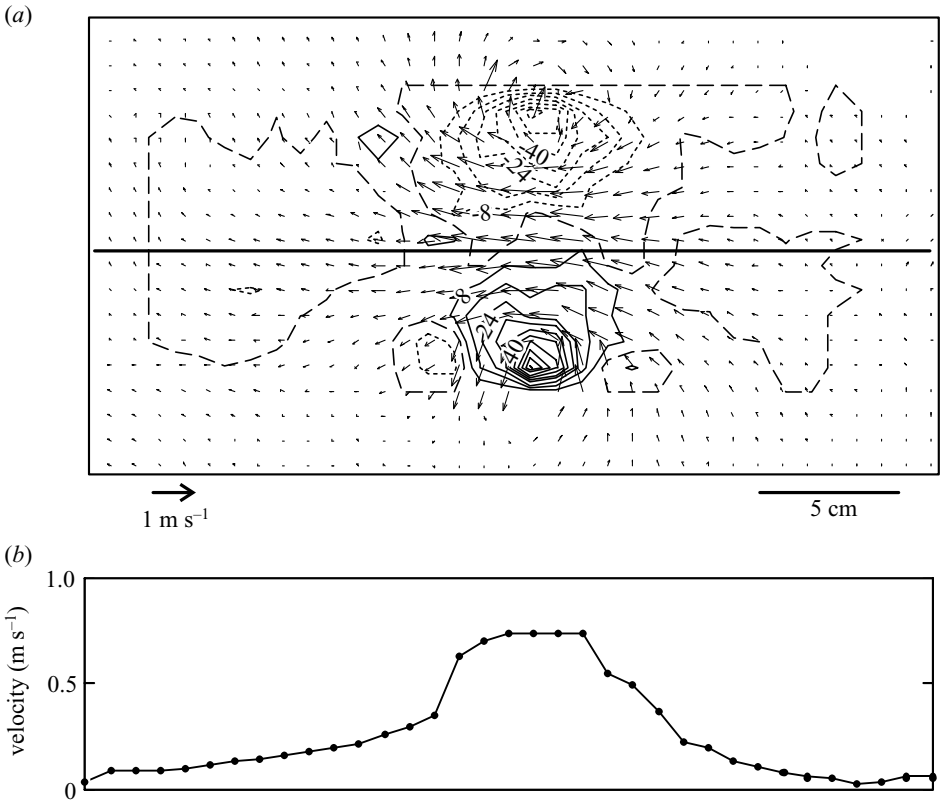

Figure 5. A sample vector field plot of a laminar vortex ring ($Re = 4700$) at $t = 0.3$ s ($t^* = 2.8 \times 10^{-5}$). The thick solid line in part (*a*) indicates the centre-line. (*a*) PIV velocity vector data with vorticity shown with contours. Solid contours indicate anticlockwise vorticity, dotted contours indicate clockwise vorticity, and the dashed contour is the 0 s^{-1} contour. The separation between contours is 8 s^{-1}. (*b*) Centre-line velocity plot, showing fluid velocity in the direction of the centre-line.

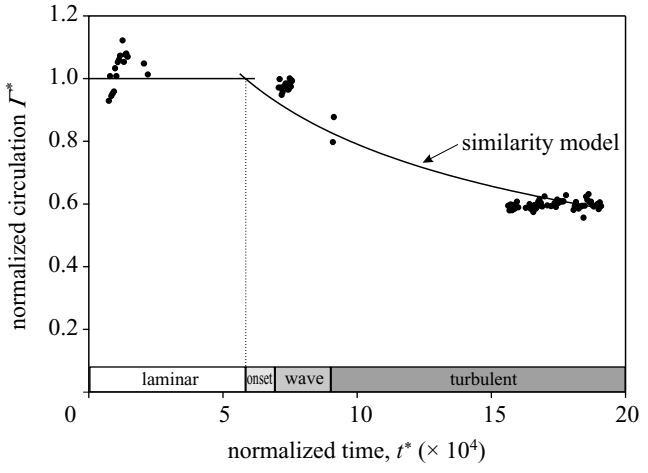

Figure 6. Normalized centre-line circulation versus time. The three clusters of points are from different rings, all with $Re = 4500$. The solid curves show the model for decay in circulation: until the onset of turbulence at $t = 1.5$ s ($t^* = 5.8 \times 10^{-4}$ s), circulation should remain constant, and after that, it falls according to the similarity model in equations (2.5) and (2.6). The bar at the bottom indicates the state of the ring, from laminar to turbulent.

mates: $x_0 = -2.3 \pm 0.3$ m and $t_0 = -0.30 \pm 0.20$ s. Based on these x_0 and t_0 values, G was estimated to be 3.8 ± 1.7. Using equation (2.7), the actual circulation can be approximated at any time; thus, extrapolating back to the onset of the wave instability at 1.5 s ($t^* = 0.0005$), the circulation was 680 ± 360 cm^2 s^{-1}, $\Gamma^* = 1.0 \pm 0.5$. The fitted model for turbulent decay of circulation is shown in figure 6.

All PIV data are summarized in table 2.

4. DISCUSSION

The purpose of this study was to analyse the dynamics of an idealized, hovering hawkmoth wake to identify problems with the analysis, and not to mimic the complexity of the real wake. Even for simple, circular, isolated vortex rings generated under controlled conditions, the transition to turbulence causes a major problem in the wake analysis. Circulation and therefore impulse estimates are robust and constant while the ring remains laminar, but shedding of vorticity after the transition to turbulence causes a sharp decline in circulation. In the controlled conditions of this study, it was possible to extrapolate back and estimate the initial circulation of a turbulent ring, but this is probably not feasible for a real wake. First, it is unlikely that the apparent turbulent origin can be determined in a real wake: accurate velocity and position measurements are difficult to make, and the turbulent transition time will be hard to estimate. Second, vortex rings in a real wake probably do not gradually make a transition to turbulence. Willmott *et al.* (1997) observed a much more rapid turbulent breakdown of vortex rings in the hawkmoth wake, apparently caused by interaction between rings; the ring created on the downstroke breaks down nearly instantaneously during supination, when the trailing vortex from the wing tip is close to the ring. Thus, turbulence seems to be triggered not by the azimuthal wave instability, but

Table 2. Summary of PIV data in the three regions.
(See text for an explanation of the calculations. The values in the parentheses are assumed and the dashes indicate parameters that had too little data to calculate.)

			region 1	region 2		region 3
			laminar	laminar	transition	turbulent
generated						
circulation	Γ_0	($cm^2\ s^{-1}$)	710	670	670	658
Reynolds number	*Re*		4700	4500	4500	4400
measured						
times	t	(s)	0.3–0.6	1.0–2.0	2.5	4.2–5.1
radius	R	(mm)	40.2 ± 0.3	42.1 ± 0.7	39 ± 1	(44)
ring circulation	Γ	($cm^2\ s^{-1}$)	729 ± 9	654 ± 9	560 ± 38	393 ± 1
estimated generation parameters						
circulation	Γ	($cm^2\ s^{-1}$)	729 ± 9	654 ± 9	—	680 ± 360

by the interaction between vortices, and the model of Glezer & Coles (1990) may not be accurate. Regardless of the model's accuracy, though, the breakdown is so rapid that it would be difficult to make measurements before the ring structure completely dissipates.

In principle, estimating circulation by the centre-line integration method should include the vorticity shed into the wake of a turbulent vortex ring. For their pigeons and jackdaws, Spedding *et al.* (1984) and Spedding (1986) compared this estimate with that obtained by the line integral around a closed loop enclosing the vortex core. They found that the core circulation was typically three-fifths of the total circulation estimated by the centre-line method, a value that is consistent with experimental studies on turbulent rings (Maxworthy 1977). About 40% of the vorticity had therefore been shed into the wake, even though it was not obvious from visual inspection of the flow visualization photographs. However, without a timed series of photographs and the benefit of the turbulent decay model of Glezer & Coles (1990), which was published later, Spedding could not estimate how the total circulation decreased with time. Some shed vorticity crosses the centre-line in the wake, and is cancelled by surrounding vorticity of the opposite sense. This leads to the observed decay of circulation and impulse with time, even using the centre-line integration method.

It is clear that measurements must be made while the wake vortices remain laminar to allow accurate estimates of circulation and impulse; otherwise, the wake is almost certain to show a momentum deficit. Furthermore, except for special cases (like the pigeon and jackdaw) where wake vortices are relatively isolated or turbulent, circulation should not be estimated by the centre-line integration method. Most wakes have a complicated three-dimensional structure, and velocities along the centre-line will also be influenced by other recently shed vortices. Circulation should be estimated instead by the line integral around a closed loop enclosing the laminar vortex core. In addition, one should not assume that the wake rings are circular; instead, the actual area of the vortex loop must be used.

Spedding's momentum deficit for the wakes of pigeons and jackdaws (Spedding *et al.* 1984; Spedding 1986) may be a result, in part, of measurements on turbulent rings. The ring Reynolds number *Re* for the vortex rings that he observed are much higher than those in this study. Ring impulse I, from equation (2.10), is equal to the ideal impulse in equation (1.1)

$$I = \pi\rho\Gamma r^2 = \frac{mg}{f}, \tag{4.1}$$

which allows us to solve for Γ and the ring *Re*

$$\Gamma = \frac{mg}{\rho\pi R^2 f} = \frac{p_d}{\rho f}$$

and

$$Re = \frac{p_d}{\rho\nu f}. \tag{4.2}$$

Thus, the ring Reynolds number in the wake of Spedding's pigeons should be *ca.* 90 000, well into the range that Glezer (1988) found to be turbulent from formation. Such turbulent rings should begin to shed vorticity immediately, possibly crossing the centre-line and being cancelled by opposing vorticity or becoming obscured by measurement error, making it difficult to detect and leading to a momentum deficit.

In general, it is probably not possible to measure wake circulation accurately for animals larger than insects or the smallest birds. Disc loading and wing beat frequency scale approximately as R and $R^{-3/4}$, respectively, for geometrically similar animals (Dudley 2000). Thus, substituting these proportionalities into equation (4.2), ring Reynolds number should be proportional to $R^{7/4}$. Given that a hawkmoth with a wing length of 5 cm has a ring Reynolds number of *ca.* 5000, a small bird with wing length of 10 cm should have *Re* near 17 000, which is at the low end of the range of vortex rings that Glezer (1988) found to be initially turbulent. For birds as large as pigeons, the vortex wake will almost certainly be turbulent from generation. Although it was possible under the controlled conditions

of this study to estimate initial circulation from a turbulent vortex ring, it will probably not be so in studies of flying animals. Thus, large insects such as hawkmoths or small birds such as hummingbirds probably represent the largest animals for which the wake circulation can be measured accurately.

This work was performed with the support of a Winston Churchill Foundation Scholarship and the BBSRC. Dr S. Dalziel of the Department of Applied Mathematics and Theoretical Physics kindly provided the loan of the laser. The authors thank R. Holder and G. Harrison, who were instrumental in the construction of the vortex ring generator, and U. Müller for guidance and support during the project.

REFERENCES

Alexander, R. M. 1997 The U, J and L of bird flight. *Nature* **390**, 13.

Casey, T. M. & Ellington, C. P. 1989 Energetics of insect flight. In *Energy transformation in cells and organisms* (ed. W. Wieser & E. Gnaiger), pp. 200–210. Stuttgart, Germany: Georg Thieme Verlag.

Dickinson, M. H., Lehmann, F.-O. & Sane, S. 1999 Wing rotation and the aerodynamic basis of flight. *Science* **284**, 1954–1960.

Didden, N. 1979 On the formation of vortex rings: rolling-up and production of circulation. *Z. Angew. Math. Phys.* **30**, 101–116.

Didden, N. 1982 On vortex formation and interaction with solid boundaries. In *Vortex motion* (ed. H. G. Hornung & E.-A. Müller), pp. 1–17. Braunschweig: Friedrich Vieweg and Sohn.

Dudley, R. 2000 *The biomechanics of insect flight*. Princeton University Press.

Ellington, C. P. 1984*a* The aerodynamics of hovering insect flight. IV. Aerodynamic mechanisms. *Phil. Trans. R. Soc. Lond.* B **305**, 79–114.

Ellington, C. P. 1984*b* The aerodynamics of hovering insect flight. V. A vortex theory. *Phil. Trans. R. Soc. Lond.* B **305**, 115–144.

Ellington, C. P., van den Berg, C., Willmott, A. P. & Thomas, A. L. 1996 Leading-edge vortices in insect flight. *Nature* **384**, 626–630.

Glezer, A. 1988 The formation of vortex rings. *Phys. Fluids* **31**, 3532–3541.

Glezer, A. & Coles, D. 1990 An experimental study of a turbulent vortex ring. *J. Fluid Mech.* **211**, 243–283.

Huang, H., Dabiri, D. & Gharib, M. 1997 On errors of digital particle image velocimetry. *Meas. Sci. Tech.* **8**, 1427–1440.

Lighthill, M. J. 1973 On the Weis–Fogh mechanism of lift generation. *J. Fluid Mech.* **60**, 1–17.

Maxworthy, T. 1977 Some experiemental studies of vortex rings. *J. Fluid Mech.* **81**, 465–495.

Nogueira, J., Lecuona, A. & Rodríguez, P. A. 1997 Data validation, false vectors correction and derived magnitudes calculation on PIV data. *Meas. Sci. Tech.* **8**, 1493–1501.

Pennycuick, C. J. 1975 Mechanics of flight. In *Avian biology*, vol. 5 (ed. D. S. Farner & J. R. King), pp. 1–75. London: Academic.

Rayner, J. M. V. 1979*a* A vortex theory of animal flight. Part 1: The vortex wake of a hovering animal. *J. Fluid Mech.* **91**, 697–730.

Rayner, J. M. V. 1979*b* A vortex theory of animal flight. Part 2: The forward flight of birds. *J. Fluid Mech.* **91**, 731–763.

Saffman, P. G. 1970 The velocity of viscous vortex rings. *Stud. Appl. Math.* **49**, 371–380.

Sallet, D. W. & Widmayer, R. S. 1974 An experimental investigation of laminar and turbulent vortex rings in air. *Z. Flugwiss.* **22**, 207–215.

Sane, S. P. & Dickinson, M. H. 2002 The aerodynamic effects of wing rotation and a revised quasi-steady model of flapping flight. *J. Exp. Biol.* **205**, 1087–1096.

Shariff, K. & Leonard, A. 1992 Vortex Rings. *Ann. Rev. Fluid Mech.* **24**, 235–279.

Spedding, G. R. 1986 The wake of a jackdaw (*Corvus monedula*) in slow flight. *J. Exp. Biol.* **125**, 287–307.

Spedding, G. R., Rayner, J. M. V. & Pennycuick, C. J. 1984 Momentum and energy in the wake of a pigeon (*Columba livia*) in slow flight. *J. Exp. Biol.* **111**, 81–102.

Sun, M. & Tang, J. 2002 Unsteady aerodynamic force generation by a model fruit fly wing in flapping motion. *J. Exp. Biol.* **205**, 55–70.

Taylor, J. R. 1982 *An introduction to error analysis*. Sausalito, CA: University Science Books.

van den Berg, C. & Ellington, C. P. 1997*a* The three-dimensional leading-edge vortex of a 'hovering' model hawkmoth. *Phil. Trans. R. Soc. Lond.* B **352**, 329–340. (DOI 10.1098/rstb.1997.0023.)

van den Berg, C. & Ellington, C. P. 1997*b* The vortex wake of a 'hovering' model hawkmoth. *Phil. Trans. R. Soc. Lond.* B **352**, 317–328. (DOI 10.1098/rstb.1997.0024.)

Weigand, A. & Gharib, M. 1994 On the decay of a turbulent vortex ring. *Phys. Fluids* **6**, 3806–3808.

Weigand, A. & Gharib, M. 1997 On the evolution of laminar vortex rings. *Exp. Fluids* **22**, 447–457.

Westerweel, J. 1997 Fundamentals of digital particle image velocimetry. *Meas. Sci. Tech.* **8**, 1379–1392.

Willmott, A. P. & Ellington, C. P. 1997*a* The mechanics of flight in the hawkmoth *Manduca sexta*. I. Kinematics of hovering and forward flight. *J. Exp. Biol.* **200**, 2705–2722.

Willmott, A. P. & Ellington, C. P. 1997*b* The mechanics of flight in the hawkmoth *Manduca sexta*. II. Aerodynamic consequences of kinematic and morphological variation. *J. Exp. Biol.* **200**, 2723–2745.

Willmott, A. P., Ellington, C. P. & Thomas, A. L. R. 1997 Flow visualization and unsteady aerodynamics in the flight of the hawkmoth, *Manduca sexta*. *Phil. Trans. R. Soc. Lond.* B **352**, 303–316. (DOI 10.1098/rstb.1997.0022.)

GLOSSARY

LVDT: linear variable displacement transducer
PIV: particle image velocimetry